Interfacial properties of gramicidin and gramicidin-lipid mixtures measured with static and dynamic monolayer techniques

H. Tournois,* P. Gieles,‡ R. Demel,* J. de Gier,* and B. de Kruijff*§

*Centre of Biomembranes and Lipid Enzymology and §Institute of Molecular Biology and Medical Biotechnology, University of Utrecht, Utrecht, The Netherlands; and ‡Department of Technical Physics, Eindhoven University of Technology, Eindhoven, The Netherlands

ABSTRACT Gramicidin films at the air/water interface are shown to exhibit a phase transition at 225 Å^2/molecule which might be caused by either cluster formation, reorientation of molecules, conformational changes or multilayer formation. It is further shown that coupling of a charged group on either NH_2- or COOH-terminus or elongation of the peptide by two amino acids, only slightly affects the surface area characteristics whereas modification of the tryptophans or even replacement of a single tryptophan by phenylalanine leads to drastic alterations in the surface-area characteristics and a (partial) loss of the phase transition demonstrating that the tryptophans play an important role in the interfacial behavior of gramicidin. The lack of a solvent history effect on the interfacial behavior indicates a rapid conformational interconversion of the peptide at the air/water interface. Gramicidin in mixtures with dioleoylphosphatidylcholine and lysopalmitoylphosphatidylcholine shows a condensing effect whereas gramicidin shows ideal mixing with dioleoylphosphatidylethanolamine. The condensing effect most likely is related to the aggregational state of the peptides which is different in phosphatidylcholines and phosphatidylethanolamines.

INTRODUCTION

Linear gramicidins are polypeptide antibiotics produced by *Bacillus brevis* (ATCC 8185) (1). These peptides have been proposed to be involved in bacterial sporulation by interaction with the transcriptional process during sporogenesis (2–5). Despite this intriguing biological function gramicidins are especially known for their ability to specifically facilitate passive diffusion of protons and alkali cations through membranes (6, 7). Furthermore gramicidins form an excellent model system for conformational studies of membrane proteins (8) and for protein-lipid interactions (9, 10). In particular the peptide has been shown to be a very potent modulator of lipid structure of which bilayer formation with lysophosphatidylcholine (LPC)[1] and H_{II} phase formation with phospholipids of an acyl chain length exceeding 16 carbon atoms are the most striking examples (see reference 11 for an overview).

The primary structure of naturally occurring gramicidins is (12, 13):

Formyl-L-X^1-gly^2-L-ala^3-D-leu^4-L-ala^5-D-val^6-L-val^7-D-val^8-L-trp^9-D-leu^{10}-L-Y^{11}-D-leu^{12}-L-trp^{13}-D-leu^{14}-L-trp^{15}-ethanolamine

X can be either valine or isoleucine and Y is tryptophan, phenylalanine or tyrosine in gramicidin A, B, and C (GR A, GR B, and GR C), respectively. All aromatic side chains are residing near the COOH-terminus of the molecule. Although gramicidins are relatively simple peptides they exhibit a complex conformational behavior and can adopt various folding motifs, depending on concentration, solvent polarity, and temperature (14–17). The molecule adopts distinctly different conformations in membranes and organic solvents (18).

The tryptophans of the peptide appear to be essential for the inhibition of RNA polymerase (2), for the channel function (19–21), and also for the lipid structure modulating ability of the peptide (22–24). It has been hypothesized (25) that the tryptophan indol rings are involved in stacking interactions which may determine the conformation of the peptide (19, 26) and are important for functional GR-protein interactions. First, replacement of trp^{11} by phe^{11} yielding GR B results in very different circular dichroism characteristics (19, 23), Tl^+ binding properties (27), and influence on lipid organization (23). It has been suggested that the $\beta^{6.3}$ helix conformation, which is thought to be the conformation which, by N-N dimerization, forms the functional channel (8, 28–30), is stabilized by stacking interactions, involving the tryptophans at position 9 and 15 (19, 26). Second, tryptophans apparently play an important role in the process of lateral self-association and are thought to stabilize (ordered) aggregate structures by intermolecular stacking interactions (31, 32). Interestingly an aggregational model for

[1] *Abbreviations used in this paper:* A, surface area; DOPC, dioleoylphosphatidylcholine; DOPE, dioleoylphosphatidylethanolamine; GR, gramicidin; GR A′, natural mixture of gramicidin; LPC, lysophosphatidylcholine; NFGR A′, Trp-*N*-formylated gramicidin A′; ϵ_d, surface dilatational elasticity; $|\epsilon_d|$, modulus of surface dilatational elasticity; ϕ_d, phase angle; η_d, dilatational viscosity; π, surface pressure; σ, surface tension; ω, angular frequency.

0006-3495/89/03/557/13 $2.00

GR was proposed to explain single channel conductance (33). In this model lateral intermolecular interactions are involved in formation of a single conducting unit. Third, the bulky tryptophan residues impose a cone shape to the molecule. The shape, in combination with the strong tendency to self associate has been used to explain the lipid structure modulating ability of the peptide (10, 31, 32). Brasseur et al. (36) calculated by conformational analysis procedures that the $\beta^{6.3}$ conformation of GR, by its shape and intermolecular interactions, is likely to form aggregate structures with a geometry matching that of the tubes found in the GR-induced H_{II} phase. Such structures are suggested to be intermediates in the gramicidin-induced H_{II} phase formation (34, 35). Aggregate formation by GR appears to be dependent on the peptide to lipid ratio and the type of lipid; for instance GR is less soluble in phosphatidylethanolamine bilayers than in bilayers of phosphatidylcholines (37, 38).

To get more insight into the relationship between the chemical structure of GR, its conformational behavior, and its intermolecular interactions, we have chosen to use the monolayer technique to study the interfacial properties of a series of GR analogues in pure form and in mixtures with those lipids in which the peptide modulates lipid polymorphism. In view of the conflicting data and interpretations of previous monolayer studies of GR in particular with respect to the orientation and molecular dimensions (39–44), we applied both static and dynamic monolayer techniques.

MATERIAL AND METHODS

Gramicidin A′ (GR A′), which is the natural mixture, was obtained from Sigma Chemical Co., St. Louis, MO, and used without further purification. Tryptophan *N*-formylated gramicidin was synthesized as described before (22). Gramicidins A, B, and C were isolated from the natural mixture according to Killian et al. (23). *N*-Succinyl-, *O*-succinyl-, and desformylgramicidin were prepared and purified as described previously (45). [phe^9]-, [phe^{11}]-, con [leu-ala]-, con [leu-trp]-, and con [leu-ala]$_2$ gramicidin (chemical structures are given in Table 1) were a kind gift of Dr. D. W. Urry. Bovine serum albumin (BSA fraction V) was purchased from Sigma Chemical Co. All peptides were checked by HPTLC (45) and found to be pure.

Concentrations of the peptide solutions were determined by weight and by quantitative amino acid analysis after hydrolysis in propionic acid/12 M HCl (1:1 vol/vol) as described previously (47). 1,2-Dioleoyl-*sn*-glycero-3-phosphocholine, 1,2-dioleoyl-*sn*-glycero-3-phosphoethanolamine, 1,2-dipalmitoyl-*sn*-glycero-3-phosphocholine, and 1-palmitoyl-*sn*-glycero-3-phosphocholine (LPC) were synthesized and purified as described before (48, 49). Lipid concentrations were determined by phosphorus analysis (50). All solvents used were of analytical grade.

Measurement of force-area isotherms

Surface pressure-area experiments were carried out at 20°C using a Teflon Langmuir trough (32.2 × 17.2 × 1.5 cm) equipped with a movable barrier. The rate of compression could be varied between 0.2 and 105 cm^2 min^{-1} but was unless otherwise stated 78.9 cm^2 min^{-1}. Surface pressure was measured with an electrochemically roughened platinum (Wilhelmy) plate (2 cm wide) and an electrobalance (model LM 500, Beckman Instruments, Inc., Fullerton, CA). Appropriate amounts of peptide, lipid, or a mixture of both, unless otherwise stated dissolved in chloroform-ethanol 1:1 (vol/vol) at a concentration of 0.1–1 mM, were spread on a subphase containing 10 mM Tris HCl (pH 7.4 in triple distilled water) with an Agla microsyringe. The tip of the syringe was mechanically lowered to contact the interface, then raised slightly so that meniscus formation occurred. The glass tip was coated with dimethyldichlorosilane (5% in chloroform) to prevent gramicidin to adhere to the tip. It was found that this treatment was essential to reproducibly spread the desired amount of peptide onto the interface. The surface pressure-area isotherms were measured at least in triplicate and were found to be reproducible within ±5 Å^2. In between measurements the surface was swept carefully at least four times. The barrier and the Wilhelmy plate were cleaned with ethanol and rinsed with doubly distilled water.

The equilibrium surface pressure, which is the pressure at which spreading of additional amounts of GR does not cause a permanent surface pressure increase, was determined by spreading small portions of peptide on a trough of fixed area until a maximal pressure was reached.

TABLE 1 Chemical structures of gramicidin derivatives

Compound		Peptide sequence 1 2 3 4 5 5a 5b 5c 5d	6 7 8 9 10 11	12 13 14 15	
Gramicidin A	F–	X-gly-ala-leu-ala.....	val-val-val-trp-leu-*trp*-	leu-trp-leu-trp-E	(12)
Gramicidin B	F–	X-gly-ala-leu-ala.....	val-val-val-trp-leu-*phe*-	leu-trp-leu-trp-E	(12)
Gramicidin C	F–	X-gly-ala-leu-ala.....	val-val-val-trp-leu-*tyr*-	leu-trp-leu-trp-E	(13)
[phe^9]-GR A	F–	X-gly-ala-leu-ala.....	val-val-val-*phe*-leu-trp-	leu-trp-leu-trp-E	(19)
desf. Gr A′	+	*X*-gly-ala-leu-ala.....	val-val-val-trp-leu-Y-	leu-trp-leu-trp-E	(12)
O-succ-GR A′	F–	X-gly-ala-leu-ala.....	val-val-val-trp-leu-Y-	leu-trp-leu-trp-E-*succ*$^-$	(45)
N-succ-GR A′	$^-$*succ*-	X-gly-ala-leu-ala.....	val-val-val-trp-leu-Y-	leu-trp-leu-trp-E	(45)
con(leu-ala)-GR A	F–	val-gly-ala-leu-ala-*leu-ala*.....	val-val-val-trp-leu-trp-	leu-trp-leu-trp-E	(46)
con(leu-ala)$_2$GR A	F–	val-gly-ala-leu-ala-*leu-ala-leu-ala*-....	val-val-val-trp-leu-trp-	leu-trp-leu-trp-E	(46)
con[leu-trp]-GR A	F–	X-gly-ala-leu-ala.....	val-val-val-trp-leu-trp-	leu-trp-leu-trp-*leu-trp*-E	—
NFGR A′	F–	X-gly-ala-leu-ala.....	val-val-val-*FT*-leu-*FT*-	leu-*FT*-leu-*FT*-E	(22)

E, ethanolamine; F, formyl; FT, *N*-formylated trp; succ$^-$, succinyl; X, val or ile; Y, trp, phe, or tyr.

Measurements of the surface dilatational elasticity and surface dilatational viscosity

The experimental system and procedure are a variant of the Benjamins-de Feyter method (51, 52) and have been described in detail previously by Boonman et al. (52, 53). An area at the air/water interface in a Teflon trough is enclosed in a rectangle formed by two rigid barriers connected by elastic ribbons perpendicular to and partially immersed in the interface. The elastic material was prepared and treated in a Soxlet containing ethanol, thus removing impurities. One of the barriers is a standard moving barrier, the other can be harmonically oscillated. This construction provides a surface with a constant width of 12.5 cm and an initial length of 22 cm. After spreading of the monolayer the surface pressure can be adjusted with the movable barrier. Small-amplitude sinusoidal waves are generated within the rectangle by harmonically oscillating the second barrier in the plane of the interface. This periodic compression-expansion at a variable frequency of 50–750 mHz subjects the monolayer to a periodic deformation ($\Delta A/A \sim 0.01$). Due to the elastic side walls which move in phase with the monolayer the imposed deformation is purely dilatational. The surface pressure was measured with a Cahn RH automatic balance and a Wilhelmy plate of filter paper (52) at a fixed position (0.423 × actual length of the film) to circumvent the need to apply corrections for inhomogeneities. Signals related to surface tension, barrier displacements, and the position of the Wilhelmy plate were monitored with a microcomputer (LSI), connected to a PDP-11/23 minicomputer for purposes of data handling. All experiments were performed at 20°C and within one experiment the temperature was constant within ±0.3°C.

Theoretical background

The theoretical basis for the calculation of viscoelastic interfacial properties by generating interfacial waves has been provided by the work of Lucassen and co-workers (54, 55). The surface dilatational elasticity, ϵ_d, can be described by Eq. 1:

$$\epsilon_d = A \cdot (d\sigma/dA), \tag{1}$$

where A is the surface area and ρ is the surface tension. Eq. 1 is valid provided that no shear forces are present in the interfacial region. In the case of a clean surface $\epsilon_d = 0$, whereas in the presence of a monomolecular layer $\epsilon_d \neq 0$.

In case of harmonic area oscillations the dilatational elasticity can be described by Eq. 2.

$$\epsilon_d = |\epsilon_d| \cdot e^{j\phi d} = \epsilon_r + j \cdot \epsilon_i, \tag{2}$$

in which $|\epsilon_d|$ is the modulus of the dilatational elasticity, $j = (-1)^{1/2}$, ϕ_d is the phase angle of the dilatational elasticity. ϵ_r and ϵ_i are respectively the real and imaginary parts of ϵ_d. ϕ_d reflects the difference in phase between the locally imposed oscillation in the surface area and the detected oscillation in the surface tension. This time lag may be caused by processes occurring at the interface like diffusion, adsorption, or the formation of aggregate structures (56). In the case of purely elastic behavior $\phi_d = 0$ which means that response to dilatation is immediate. The viscoelastic behavior in case of harmonic variations in A can be described as

$$\epsilon_d = \epsilon_r + j\omega\eta_d, \tag{3}$$

in which ω is the angular frequency and η_d the dilatational viscosity.

The value of $|\epsilon_d|$ can be determined from the amplitudes of the harmonic oscillations of A and σ, ΔA and $\Delta\sigma$ using Eq. 3:

$$|\epsilon_d| = A_0 \cdot (\Delta\sigma/\Delta A), \tag{4}$$

in which A_0 is the initial area at $\Delta A = 0$. Eq. 3 is valid when satisfying the condition $kL \ll 1$ (54) with k being the wave number of the longitudinal wave and L the length of the monolayer in the direction of the wave propagation. The loss-angle, ϕ_d, can be calculated from the difference in phase between $\Delta\sigma$ and ΔA. The occurrence of relaxation in or near the surface after distortion of the film gives rise to a viscous component ($j\omega\eta_d$) which determines the dissipation of energy in the film

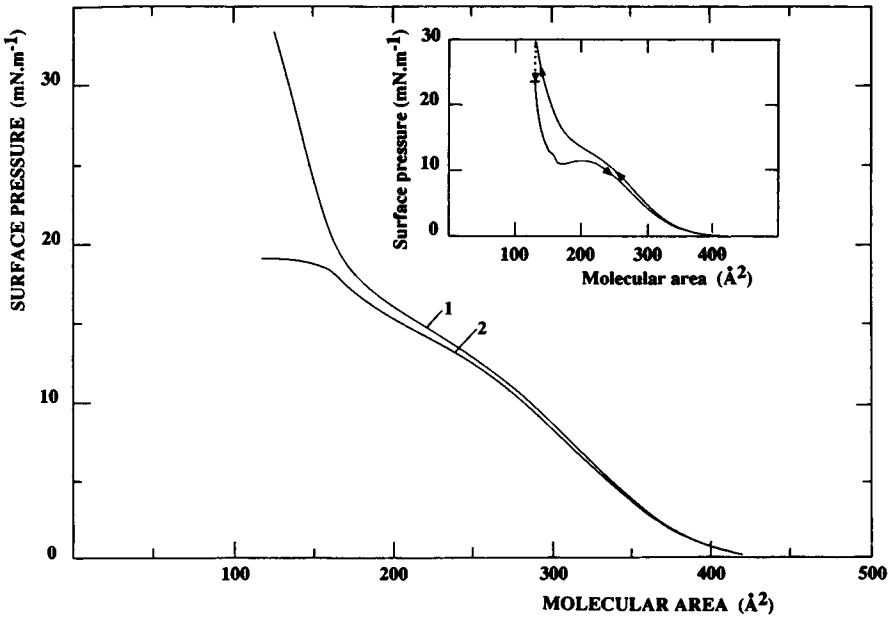

FIGURE 1 Pressure-area isotherms of gramicidin (*1*) measured by continuous compression and (*2*) by stepwise compression and relaxation. Insert shows the hysteresis effect encountered when the film is expanded after compression and 4 min relaxation.

(54). For practical reasons we will be dealing with ϕ_d instead of η_d as a parameter for (visco)-elastic mechanical properties.

RESULTS

Pure peptides

A typical surface pressure–area isotherm obtained for GR A′ at the air-water interface by continuous compression (78.9 $cm^2 \cdot min^{-1}$) is shown in Fig. 1 (*curve 1*). On compression a first increase in surface pressure is observed at a molecular area of 420–430 $Å^2$ and the curve is characterized by a deflection at a molecular area of ~280 $Å^2$ (~10–12 $mN \cdot m^{-1}$). At ~12–15 $mN \cdot m^{-1}$ the compressibility of the film is largely increased until an area of ~180 $Å^2$/molecule is reached. Continuing compression results in a steep increase in surface pressure. Here the monolayer becomes highly imcompressible and visually rigid; it ceases to flow and the Wilhelmy plate is displaced from its vertical orientation. At continuous compression, the sharp increase in surface pressure is approximately linear up to 50–55 $mN \cdot m^{-1}$ and the curve deflects above this pressure, indicating a film collapse (data not shown). The π-A characteristics of GR A′ were found to be independent of the compression rate (0.166–87.2 $Å^2 \cdot molecule^{-1} \cdot min^{-1}$:0.2–105 $cm^2 \cdot min^{-1}$) and also independent of the solvent from which GR A′ (0.5 mM) was applied to the surface (DMSO, trifluoroethanol, ethanol, methanol, chloroform-ethanol 1:1 (vol/vol)).

When the compression is stopped at pressures above 20 $mN \cdot m^{-1}$, relaxation is observed. Equilibrium is reached only after several hours at 18–20 $mN \cdot m^{-1}$. The kinetics of this relaxation are dependent on the rate at which the film was compressed (range: 0.166–87.2 $Å^2 \cdot molecule^{-1} \cdot min^{-1}$). A high compression rate corresponds with a fast relaxation (data not shown). It is interesting to note that expansion of surface area at 30 $mN \cdot m^{-1}$ (after a 4-min relaxation period) reveals a very strong hysteresis of the surface pressure behavior (Fig. 1, *insert*) although

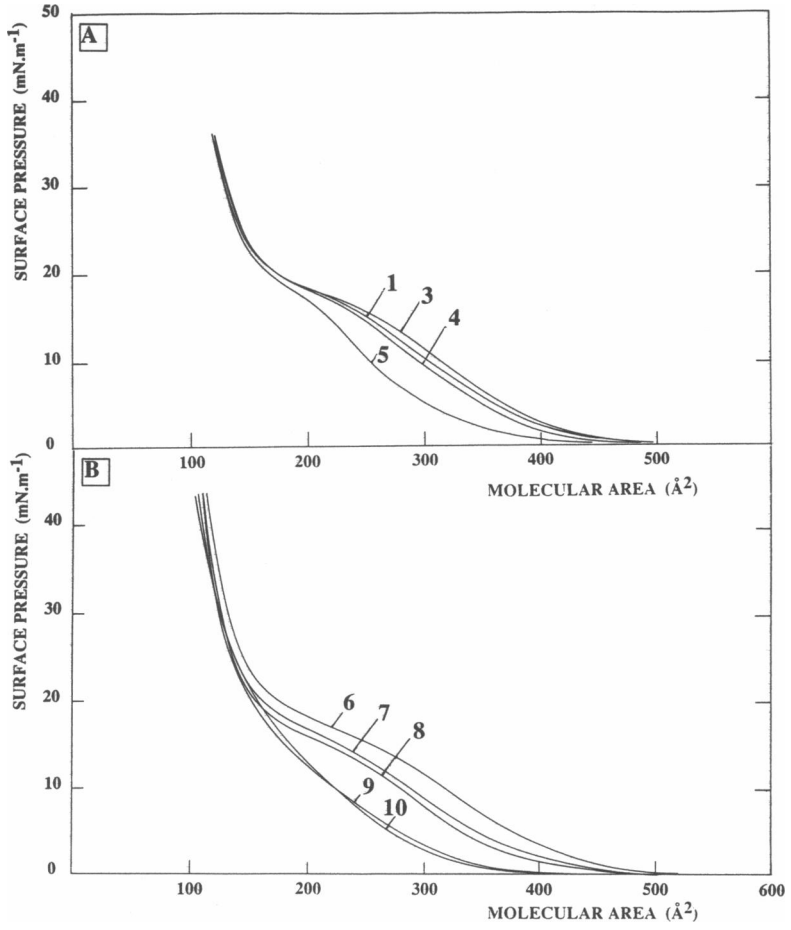

FIGURE 2 Pressure-area curves (*A*) of GR A′ (*1*), GR A (*3*), GR C (*4*), and GR B (*5*), and (*B*), of *N*-succ-GR A′ (*6*), *O*-succ-GR A′ (*7*), desf GR A′ (*8*), [phe^9]-GR A (*9*), and NFGR A′ (*10*).

no appreciable amount of material is lost from the interface as judged by recompression. The extent of this hysteresis (defined as the area between the compression and expansion curves) increases with a decreased rate of compression and prolonged relaxation (keeping the expansion rate constant 87.2 $Å^2 \cdot$ molecule$^{-1} \cdot$ min^{-1}).

A curve comparable with that obtained by continuous compression (*curve 1*) is observed by stepwise compression (compression rate 78.9 $cm^2 \cdot min^{-1}$ and applying steps of 21 cm^2) (data not shown). On ceasing compression at pressures exceeding 10 mN $\cdot$ m^{-1}, the film pressure relaxes somewhat (2–3 mN $\cdot$ m^{-1} over a period of minutes) however at pressures beyond the equilibrium surface pressure (20 mN $\cdot$ m^{-1}) a relaxation to this pressure is seen which can take 5–20 h. When allowing relaxation after each compression step to reach a stable surface pressure (the change in pressure being <0.05 mN $\cdot$ $m^{-1} \cdot min^{-1}$), π-A curve 2 (Fig. 1) is obtained. The pressure at equilibrium reached in this way, ~19 mN $\cdot$ m^{-1} is comparable with the equilibrium surface pressure. The molecular area obtained from GR π-A curves at equilibrium surface pressure was found to be 172 ± 10 $Å^2$.

Fig. 2 *A* shows π-A isotherms obtained for gramicidins, A, B, and C compared with that of GR A′ and Fig. 2 *B* obtained for various chemically modified or (semi) synthetic gramicidins. The chemical structures of these compounds are given in Table 1. It is remarkable that despite the extended range of chemical modifications the π-A curves of all peptides at higher pressures converge. The main differences are expressed in the low-pressure regions of the curves. Whereas GR A (*curve 3*) and GR C (*curve 4*) exhibit comparable π-A curves as GR A′ (*curve 1*) and have similar surface areas at both low and high pressures, GR B (*curve 5*) and the synthetic [phe^{11}]-GR (not shown) have π-A curves with only a shallow shoulder and with much smaller molecular areas at low surface pressures (Table 2). Synthetic GR A has surface characteristics similar but shifted to slightly larger area as compared with GR A which has been isolated from the commercial compound (Table 2).

TABLE 2 Molecular areas of natural occurring gramicidins and various gramicidin derivatives measured arbitrarily at 10 and 20 mN.m^{-1}

Analogue	Mol area ($Å^2$)	
	10 mN.m^{-1}	*20 mN.m^{-1}*
Gramicidin A′	305	172
Gramicidin A	314	180
Gramicidin B	252	170
Gramicidin C	295	180
Synt. GR A	330	200
[phe^9]-GR A	230	162
O-succ-GR A′	295	162
N-succ-GR A′	325	180
desf-GR A′	280	152
con[leu ala]-GR A	320	220
con[leu ala]$_2$-GR A	475	360
con[leu trp]-GR A	325	210
NFGR A′	230	152

The GR analogues with ionizable groups (Fig. 2 *B*): *N*-succ-GR A′ (*curve 6*), *O*-succ-GR A′ (*curve 7*), and desf-GR A′ (*curve 8*), also show π-A characteristics comparable with GR A′ with only slight variations in the area/molecule at lower pressures (Table 2). The negatively charged *O*-succ-GR A′ and *N*-succ-GR A′ show slightly larger areas at low surface pressures than GR A′ whereas the positively charged desf-GR A′ exhibits a more condensed curve at low pressures. However despite the presence of the ionizable groups, the π-A curves converge at higher pressures. An interesting difference in the force-area curves is observed for the derivative with a phe residue at position 9 (*curve 9*) and with formylated trp residues (*curve 10*). The lower pressure part of the curves (<20 mN $\cdot$ m^{-1}) is shifted to a smaller molecular area and the shoulder at a molecular area of 280 $Å^2$ is absent. Interestingly the expansion curves of NFGR A′ also show the characteristic 'dip' (data not shown).

The data so far suggest differences in molecular conformation or intermolecular interactions upon changes in the aromatic residues. The curve for [phe^{11}]-GR (GR B, *curve 5*) shows a small shoulder (at 15–17 mM $\cdot$ m^{-1}), whereas the curve for [phe^9]-GR (*curve 9*) does not. This difference indicates that the position of the substitution is of influence on the interfacial properties of the peptide.

In Fig. 3 force-area isotherms are shown, obtained for gramicidin analogues in which the central region is

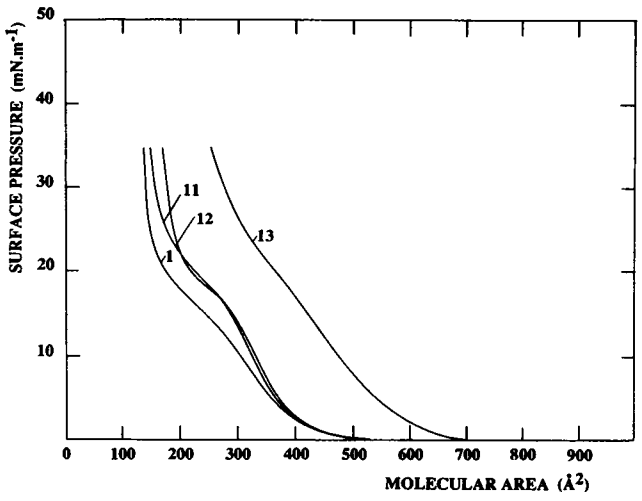

FIGURE 3 Pressure-area curve of GR A′ (*1*), con[leu-ala]-GR A (*11*), con[leu-trp]-GR A (*12*), and con[leu-ala]$_2$-GR A (*13*).

extended by two or four amino acids. The molecular area seems slightly dependent on the length of the molecule; con[leu-ala]- and con[leu-trp]-GR have slightly larger areas as compared with GR A' at both low and high surface pressures (Table 2) but are comparable with that of synthetic GR A. The π-A isotherms of these elongated gramicidins also exhibit an overall shape similar to that measured for GR A': a smooth increase in surface pressure up to 12 mN · m^{-1} followed by a plateau between 12 and 17 mN · m^{-1} and a steep increase at still higher pressures. In contrast con[leu-ala]$_2$-GR clearly has a different π-A curve with larger areas than those of synthetic and natural GR A.

To study the rheological properties of the peptide we applied dynamic monolayer techniques which can provide additional information on the molecular interactions (56–59). The moduli of surface dilatational elasticity of GR A' and several derivatives as a function of the surface pressure, measured at a compression-expansion frequency of 500 mHz, are shown in Fig. 4. As a reference bovine serum albumin (BSA) was measured because the surface rheological behavior of this protein has been studied extensively (57–59). BSA shows an elasticity increase with surface pressure reaching a plateau at ~10 mN · m^{-1}. The $|\epsilon_d|$ values obtained for BSA are comparable with those reported earlier (57–59). At low surface pressure the $|\epsilon_d|$ of the GR A' film increases with the surface pressure reaching a first maximum at 10 mN · m^{-1}. Increasing the surface pressure further, there is first a decrease in $|\epsilon_d|$ followed by a steep increase at pressures above 15 mN · m^{-1}, which coincides with the increase in the force area isotherm near the limiting area. At a surface pressure of 25 mN · m^{-1} and frequency of 500 mHz, $|\epsilon_d|$ reaches a value of 200 mN · m^{-1}. A similar behavior is observed for GR A and GR C (Fig. 4 *B*). GR B however does not show the marked increase in $|\epsilon_d|$ at high surface pressures and reaches an elasticity of only 60 mN · m^{-1} at a surface pressure of 20 mN · m^{-1} (Fig. 4 *B*). NFGR A' shows a remarkably different elastic behavior. At surface pressures exceeding 10 mN · m^{-1} an increase in $|\epsilon_d|$ up to 300 mN · m^{-1} is observed which is nearly twice the maximal value obtained for GR A' indicating much stronger interactions in the plane of the NFGR A' monolayer. This, and the higher compressibility are most likely the result of a more extensive lateral aggregation of this compound which is in agreement with earlier observations (23). Although the π-A curves of NFGR A' and GR B suggest that both compounds show a comparable deviation from GR A', the surface rheological data clearly reveal that both show in fact a very different behavior. The GR B film is a very weak one in which the molecules are unable to form a coherent film. This difference is also reflected in the aggregational behavior of GR B (23).

Fig. 5 shows the viscous phase angle ϕ_d obtained from GR A' and several derivatives as a function of the surface pressure, measured at a barrier frequency of 500 mHz. Upon increasing surface pressure, the ϕ_d of the GR A' film increases considerably up to 20° (π = 17.5 mN · m^{-1}) to decrease again at still higher pressures. A similar behavior is observed for NFGR A', however in this case a maximal ϕ_d of 22° is reached at 10–12 mN · m^{-1}. For both GR A' and NFGR A' this point of deflection corresponds to a molecular area of ~225 Å^2 (Fig 2 *B*).

GR B films show a less pronounced surface pressure dependence of ϕ_d as compared with GR A'. A maximal ϕ_d

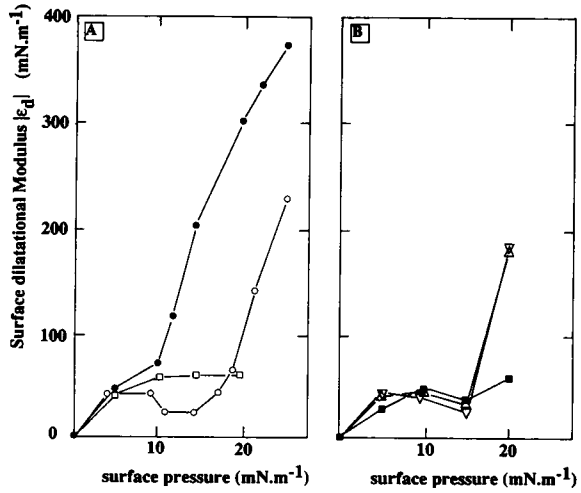

FIGURE 4 Surface dilatational modulus $|\epsilon_d|$ measured at 500 mHz as a function of the applied surface pressure (*A*) of GR A' (○), NFGR A' (●), and BSA (□), and (*B*) of GR A (△), GR C (▽), and GR B (■).

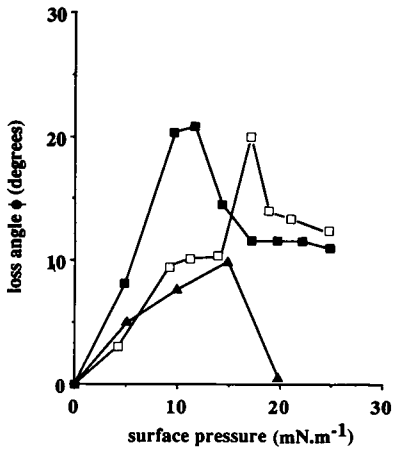

FIGURE 5 Surface dilatational loss angles measured at various surface pressures at a compression-expansion cycle frequency of 500 mHz for GR A' (□), NFGR A' (■), and GR B (▲).

of ~9° is observed at 15 mN · m^{-1}, again corresponding to a molecular area of 225 Å^2.

Because in principle the asymmetric Benjamins-De Feyter method, in which the deformation enforced on the monolayer is not purely dilatational, provides only an estimate of the real dilatational elasticity, measurements of surface viscoelastic parameters of GR A′ and its formylated analog were performed as a control using the symmetric variant of the Benjamins-De Feyter method (51). These measurements gave essentially the same results as the asymmetrical method (data not shown).

Peptide-lipid systems

In view of the differences in GR A′-lipid interactions reported for phosphatidylcholines, phosphatidylethanolamines, and lysophosphatidylcholines, it is of interest to compare the interactions between GR and different lipids by recording π-A curves of various mixtures. Fig. 6 shows, as an example, a series obtained for GR-DOPC mixtures in which the film composition is varied. It is noteworthy that the characteristic shoulder of GR is detectable above 50 mol% peptide/DOPC, indicating comparable surface behavior of GR with respect to conformation and orientation as in the absence of lipid. At lower GR fractions the π-A curves are dominated by the lipid. Above 50 mol% GR/DOPC, the mixed film at high pressures visually show a very rigid behavior comparable with the pure GR film.

The mean molecular areas of DOPC/GR films at 5, 15, and 30 mN · m^{-1} are given in Fig. 7 *A* as a function of the film composition. An ideal mixing is observed up to 20–30 mol% gramicidin. Above this a slight condensing effect is visible which increases with pressure and diminishes at higher GR mole fractions (maximal at 50–70 mol%). Essentially the same results were obtained with Egg-PC instead of DOPC (data not shown).

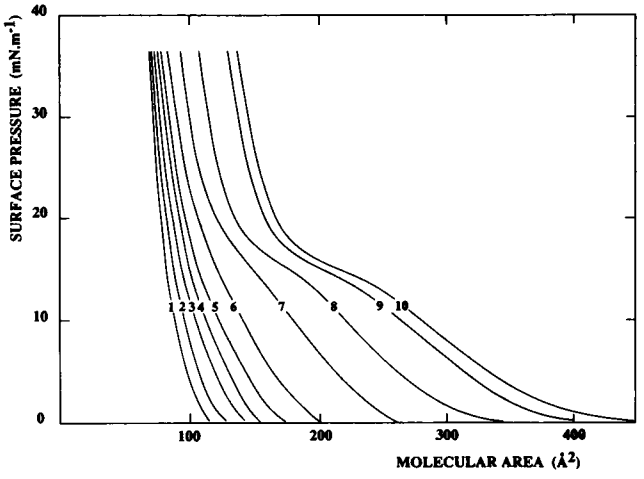

FIGURE 6 Pressure-area curves of DOPC, GR A′, and various DOPC/GR A′ mixtures. For clarity only part of the curves that are recorded is shown symbols indicate: 0 (*1*), 10 (*2*), 20 (*3*), 30 (*4*), 40 (*5*), 50 (*6*), 60 (*7*), 70 (*8*), 90 (*9*), 100 (*10*) mol% GR in DOPC.

Despite the large differences in π-A curves of GR and NFGR A′ both peptides showed a similar mixing behavior (Fig. 7 *B*). In contrast, mixtures of GR A′ with DOPE, in which GR is known to aggregate much more readily (37), showed no deviation from ideal behavior in that no significant condensing effect was detectable (Fig 7 *C*). Also NFGR A′ does not show a condensing effect in this lipid system (data not shown). 16:0 Lyso-PC forms stable films at the air-water interface. GR A′ induces a reduction in mean molecular area. The maximal effect is however shifted to lower mol% (~10–20) as compared with DOPC (Fig. 7 *D*).

Fig. 8 *A* shows the surface dilatational elasticity modulus $|\epsilon_d|$ of GR A′-DOPC mixtures at 500 mHz as a function of the surface pressure. For pure lipids this dependence is linear up to 20 mN · m^{-1}. Introduction of GR A′ (<50 mol%) causes a significant decrease in $|\epsilon_d|$ to values lower than both the pure components, implying an interaction between GR and lipids. At higher mol% of GR A′ the $|\epsilon_d|$ approaches that of the pure GR A′ film. The phase angle for pure DOPC is small (~8°) and reduces somewhat at higher surface pressures (to 3°). Addition of GR A′ leads to a considerable increase in ϕ_d reaching a maximal value (22°) at 17–20 mN · m^{-1} (Fig. 9 *A*).

Comparable data were obtained for NFGR A′-DOPC mixtures (Fig. 8 *B*), however the latter data show an increase in $|\epsilon_d|$ and a maximal ϕ_d at lower surface pressures and peptide fractions as compared with GR A′-DOPC mixtures (Fig. 9 *B*) in agreement with a more extensive lateral aggregation.

Pure DOPE films have an $|\epsilon_d|$ comparable with that of DOPC films and addition of GR leads to a comparable decrease in $|\epsilon_d|$ of the DOPE/GR monolayer to a value smaller than that of both pure DOPE and GR A′ films (data not shown). Despite the observed differences in condensing effect induced by the peptide in both lipids, the π-$|\epsilon_d|$ as well as the π-ϕ relations in these mixtures do not reveal any significant difference.

DISCUSSION

Interfacial properties of gramicidin have been studied earlier (39–44). However, although the reported force-area curves show the same features, to date no clear consensus interpretation of the monolayer behavior of GR has evolved. The reported area per molecule before collapse varies from 130–150 (39–43) to 250 Å^2/molecule

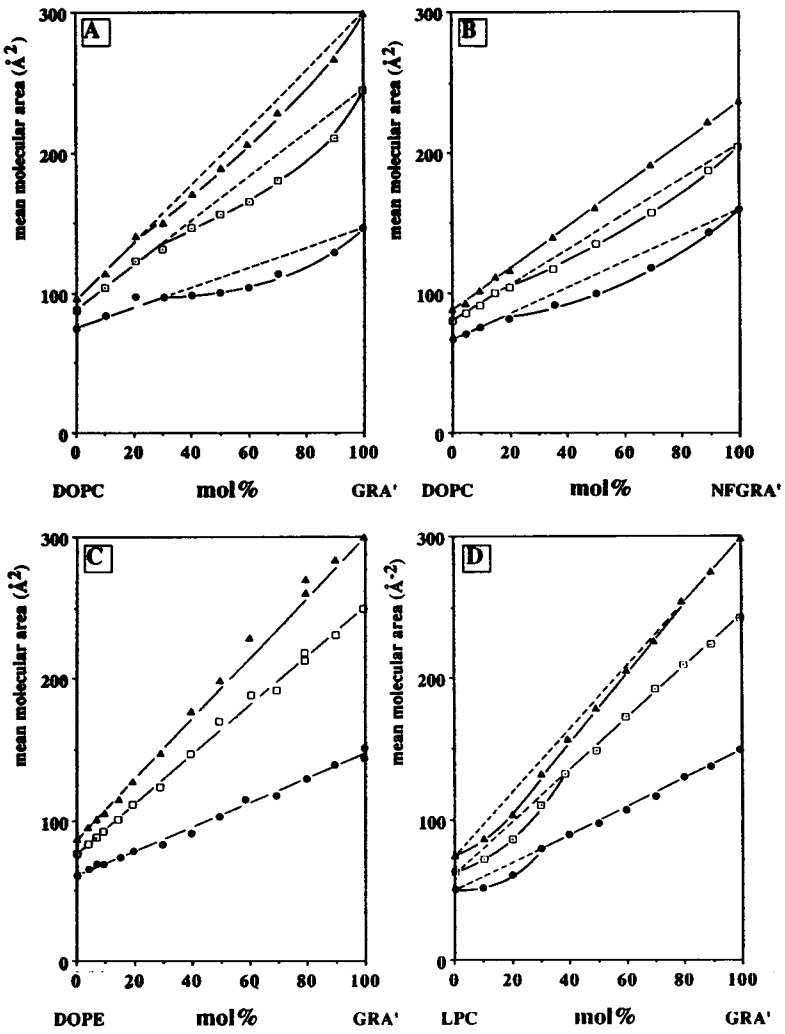

FIGURE 7 The mean molecular areas of (*A*) DOPC/GR A, (*B*) DOPC/NFGR A', (*C*) DOPE/GR A' and (*D*) LPC/GR A' mixtures at 5 (▲), 15 (□), and 30 (●) mN · m^{-1}. Dashed lines indicate the expected relation on ideal mixing.

(44). Closely related to this ambiguity, reported data for collapse of the film vary from 10 mN · m^{-1} (41) to as high as 55–60 mN · m^{-1} (43). This is to a large extent due to the different definition of the collapse pressure but might in addition be related to the strong hysteresis in the π-A behavior as documented in this study. An additional potential cause of the variation in the reported π-A curves of GR we noted is the evaporation of solvent and the adherence of peptide to the syringe tip used to apply the material to the interface. This can cause large variations in the π-A curves and will result in an underestimation of the molecular area. Coating the tip was instrumental in obtaining reproducible π-A curves.

The GR π-A curve shows a characteristic shoulder at 12–15 mN · m^{-1} indicating a transition in the molecular packing. It has been implied that this deflection of the π-A curve corresponds to the collapse of the film (41, 44). However the equilibrium surface pressure (18–20 mN · m^{-1}) as well as the pressure (20 mN · m^{-1}) obtained by relaxation of the film after compression to 30 mN · m^{-1} are higher than that at which the deflection occurs, which strongly suggests that no collapse of the film occurs at this point. Furthermore in the case of NFGR A', where there is no shoulder in the π-A curve, the equilibrium surface pressure and the pressure after relaxation are comparable with that obtained for GR A' (21 mN · m^{-1}). The present data indicate the occurrence of a transition from a loosely packed phase (280 $Å^2$/molecule) to one with a more condensed state (172 $Å^2$/molecule). A deflection in the elasticity increase with surface pressure, coinciding with a maximum loss angle, has been shown to correspond with the known phase transition in the case of phospholipids

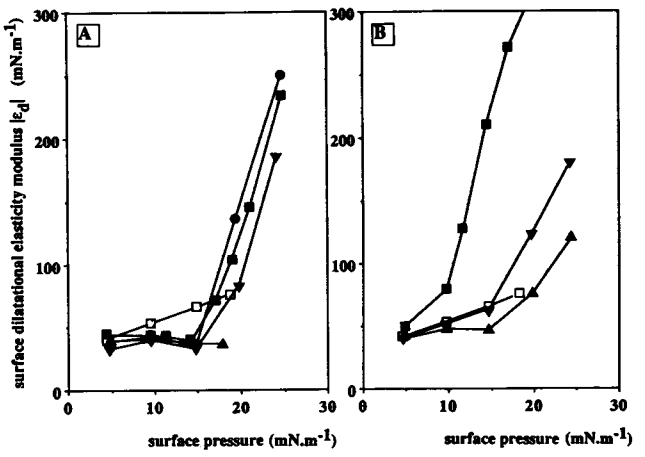

FIGURE 8 Moduli of dilatational surface elasticity as a function of the surface pressure obtained for (*A*) DOPC/GR A′ and (*B*) DOPC/NFGR A′ mixtures at 500 mHz. Used mol% peptides were: 0 (□), 50 (▲), 75 (▼), 90 (●), and 100 (■).

(52). The phase transition in the GR film, as accurately inferred from the maximum in π-ϕ, occurs at 17.5 mN · m^{-1} corresponding to a molecular area of ~225 Å^2. The decrease in phase angle at pressures above 17.5 mN · m^{-1} indicates the presence of a tightly packed state (52). In this state the molecular area is ~172 Å^2/molecule which is in reasonable agreement with earlier data (39–43). The onset of the transition occurs at much lower pressures. At 10 mN · m^{-1}, well below the actual transition, surface potential measurements of the GR film have been shown to exhibit a small nick (39, 44). The occurrence of this nick coincides with the first maximum in the $|\epsilon_d|$ (Fig. 4). Interestingly, when this change takes place, the loss-angle and thereby the viscosity of the film increase strongly.

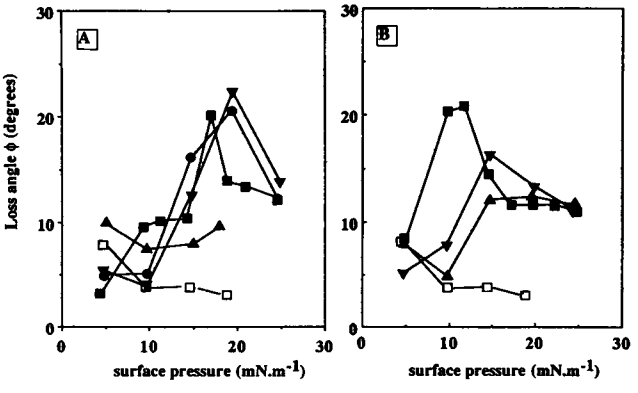

FIGURE 9 Surface dilatational loss angles ϕ_d measured at various surface pressures and for various DOPC/GRA′ (*A*), and DOPC/NFGR A′ (*B*) mixtures at 500 mHz. Used mol% peptides were: 0 (□), 50 (▲), 75 (▼), 90 (●), and 100 (■).

The course of events can be the result of several mechanisms, e.g., the formation of closely packed clusters, the transition from a (single-stranded) monomeric to a (double-stranded) dimeric molecular conformation or other conformational changes, the reorientation of the molecules from parallel to perpendicular with respect to the interface, or the formation of multilayered structures as suggested by Malcolm (60) for hydrophobic synthetic peptides. The very long relaxation times at high pressures might indicate long-lived conformational states, slowly changing towards equilibrium. It is known that GR adopts a conformational equilibrium depending on the polarity of the solvent (15–17). Recently it was shown that the solvent history of the molecule determines the conformation which it adopts upon incorporation in a membrane (61, 62). Surprisingly, addition to the interface of GR from various solvents did not show any effect on the π-A behavior. This indicates that there is a rapid conformational interconversion at the interface at low pressures.

Space-filling models of double-stranded (ds) helices like ds β^6 and ds β^7 predict molecular areas of 100 and 150 Å^2 in a perpendicular orientation (15). Analogously, models of single-stranded (ss) helices like ss $\beta^{4.4}$ and ss $\beta^{6.3}$ predict 150 and 215 Å^2/molecule, respectively (7, 14). However upon close packing the molecular areas can overlap and thereby reduce drastically. For GR in a closely packed pentameric array of ss $\beta^{6.3}$, from the data of Brasseur et al. (36), we calculated an area of 162 Å molecule. On the mere basis of these theoretical surface areas we cannot conclude which mechanism for the phase transition is correct.

In the present study we show substantial differences in π-A characteristics between the various GR derivatives upon tryptophan modification or replacement. Most surprising however, is the approximately equal limiting area of the various analogues. Even derivatives of GR with a charge on either NH_2- or COOH-terminus of the molecule exhibit similar π-A isotherms as GR, meaning that this charge does not lead to a different orientation or that the orientations, e.g., NH_2, or COOH-terminus immersed in the subphase occupy a same molecular area. In this context it is interesting to note that the elongated GR derivatives con[leu-ala]-GR A and con [leu-trp]-GR A have molecular areas that are only slightly (~20 Å^2 at 20 mN · m^{-1}) larger than that of GR A′. They were however found to be comparable with that of synthetic GR A. In fact, in general the synthetic compounds were found to have slighly larger molecular areas than their natural analogues. The reason for this is not known. The lack of large differences in molecular area of the length analogues implies a perpendicular orientation with respect to the interface for all derivatives. For gramicidin A, Brasseur calculated that if a $\beta^{6.3}$ helix were the conformation

of gramicidin at the air-water interface, the peptide would adopt a perpendicular orientation with respect to the interface (36, 63). It is of interest in this context to note that Kemp et al. (39) reported an interfacial area for the malonylbisdesformyl gramicidin dimer that equals that of GR, also suggesting a vertical orientation for both dimer and monomer of GR. It is however important to realize that con $[leu\text{-}ala]_2$-GR as an exception has much larger molecular areas as compared with GR, which is also found to be true for the retro-GR dimer as reported recently (44). These derivatives do not readily fit in the idea of a vertical orientation. We have to keep in mind that in addition to the larger molecular areas these derivatives have distinctly different π-A curves as compared with GR A. The con $[leu\ ala]_2$-GR analogue which is 19 amino acids long and the retro GR dimer, which is twice as long as GR, might adopt different conformations or orientations than GR analogues in general. A perpendicular orientation is contradictory to the parallel orientation of helices proposed by Davion-Van Mau (44) on basis of the collapse at 200–250 Å/molecule found for GR A, GR T $[tyr^{9,11,13,15}]$-GR and GR M-$[phe^{9,11,13,15}]$-GR. As discussed above, in our opinion the reported deflection in the GR curve is not a collapse but a transition encountered in most GR derivatives at ~250 $Å^2$/molecule.

Although on the basis of the present data no final conclusion can be drawn concerning the orientation of GR at the air-water interface, our data are consistent with a perpendicular orientation at all pressures.

From the present data it is clear that the tryptophan residues play an important role in the interfacial behavior of GR: replacement of trp by phe at position 9 (yielding $[^9Phe]$-GR A) or formylation of all four trp's (NFGR A') leads to a drastic reduction of the molecular area at low pressures and a disappearance of the phase transition, whereas substitution of trp^{11} by phe results in a partial loss of the deflection in the π-A curve. The fact that $[phe^9]$-GR A lacks the typical shoulder found in GR B and synthetic $[phe^{11}]$-GR could mean that the trp stacking interactions between trp^9 and trp^{15} are involved in the phase transition. Trp-trp stacking interactions have been suggested to stabilize molecular (19) as well as supramolecular structures (31, 32). Our data are consistent with this idea in that modifications that are expected to alter the aromatic–aromatic interaction forces directly or via a difference in the resulting conformation, influence the interfacial behavior. The rheological data show clear differences between GR A' and NFGR A' in that NFGR A' forms stronger films with higher elasticity, suggesting stronger intermolecular forces in the latter case which may be attributed to an increase in the dipolar moment of the tryptophan groups upon formylation. In this context it is also interesting to note that it was shown recently (44) that the π-A curves obtained for GRT and a derivative GRT' in which all tyr residues are blocked with an *O*-benzyl group, show comparable differences as observed between GR A' and NFGR A' in the present study, the GRT' having a smaller molecular area at low surface pressures than GRT despite the coupled *O*-benzyl groups.

In our opinion, there are roughly two groups of GR derivatives. One group (I) shows large molecular areas at (arbitrarily) 10 $mN \cdot m^{-1}$ (>280 $Å^2$) and a characteristic phase transition, whereas the other group (II) has smaller molecular areas (<230 $Å^2$) and lack the transition. The surface area at transition (225 Å/molecule) corresponds well with the dimensions of the $\beta^{6.3}$ helix. At higher pressures all π-A curves converge to equal surface areas, suggesting a common state of conformation and orientation. In group I a transition to this state takes place whereas in the case of group II the conformation or orientation is preexisting or the transition occurs at much lower pressures. A possibility is that the transition occurs from a ss β to an as yet unknown (possibly ds β) conformation at higher pressures. Such a transition, if occurring, seems to depend on the stability of the ss β helix and thus on the stacking interactions. The two categories proposed here might represent the same groups as recently reported by Davion-Van Mau et al. (44), which were shown to have distinctly different surface potentials and single-channel characteristics. We cannot exclude the other possibilities that the transition is caused by either cluster formation of tightly packed immobilized ss β helices resulting in a two-dimensional lattice or the formation of multilayers of gramicidin molecules which has been shown to cause comparable deflections in the π-A isotherms of a number of synthetic polypeptides (60).

To further understand GR-lipid interactions, we studied monolayers of lipid-GR mixtures. It has been established that GR induces bilayer structures in LPC, which forms micelles on its own upon hydration. The GR/LPC complexes are known to have a stoichiometry of 1/4 (24, 64) or, probably depending on the conformation of the peptide, of 1/8–10 (31). ^2H NMR studies on ^2H-labeled LPCs (66) and on ^2H-labeled GR (65), suggested a strong aggregation of GR in LPC resulting in a rigid two-dimensional GR lattice in which the interstitial spaces are filled with fluidlike lipids (65). Our present data are consistent with the formation of such aggregates with a 1:4 GR/LPC stoichiometry. At low concentrations GR dissolves well in LPC and causes a considerable condensing effect which is maximal at 10–20 mol%. At higher mol% gramicidin aggregates and becomes less efficient in its condensing effect.

GR also causes a considerable condensing effect in PC (DOPC, Egg-PC) mixtures which is maximal at ~60 mol%, in agreement with earlier data (42). However, in

contrast to these earlier data, condensing was never observed at GR A′ fractions <20 mol%, which makes this effect in DOPC less well understood. At low ratios (<1:15 mol/mol) GR is known to be well soluble in DOPC liposomes (34). However, at higher ratios sucrose gradient centrifugation of GR/DOPC mixed liposomes revealed massive aggregation of gramicidin (23) and in agreement, differential scanning calorimetric measurements of GR/dipalmitoylphosphatidylcholine (DPPC) and GR/dielaidylphosphatidylcholine (DEPC) mixtures indicated an extensive self association of the peptide at ratio's exceeding 1:15 mol/mol (37). NFGR A′ causes a comparable condensing effect in DOPC monolayers. Interestingly NFGR A′ has also been shown to exhibit a comparable or even stronger self-association behavior as GR as was inferred from the comparable (loss of) influence of the peptides on the enthalpy of the main transition of DPPC (24) and the observed aggregational behavior in DOPC multilayers with sucrose density gradient centrifugation (23). Possibly also in GR/ and NFGR A′/DOPC monolayers peptide molecules are aggregated in an extended two dimensional lattice in which the lipids can fill interstitial spaces.

In contrast GR A′-DOPE and NFGR A′-DOPE mixtures indicate ideal mixing at all fractions, which suggests different characteristics of GR A′-DOPC and -DOPE mixtures. This corresponds well with the observed differences in aggregational behavior of GR in PCs as compared with PEs (37, 38). The aggregation of GR in DEPE was proposed to be more extended due to a lesser solubility of the peptide in this lipid (37). In DOPC, due to the less extensive aggregated state of the peptide molecules, the lipid is more likely to move between the peptides than in the case of DOPE and consequently will result in a condensing effect. Remarkably the viscoelastic properties of the GR-DOPC and -DOPE mixtures are comparable and do not detect this difference in interaction. It should however be noted that also for the pure lipids, where large differences in intermolecular interactions exist between PE and PC, the elasticity measurements did not reveal any differences (data not shown).

It has been shown that the H_{II} phase inducing ability of natural gramicidins in DOPC is in the order GR A > GR A′ > GR C ≫ GR B (23, 24). A comparable sequence was found for the channel function (19). *O*-Succ-GR, *N*-succ-GR, and desf GR are approximately equally potent modulators of lipid structure as GR A′ (45). [phe^9]-GR is in this respect comparable with GR B (23). The formylated GR derivative does not induce H_{II} phase formation (22). The present data show a very good correlation between the H_{II} phase promoting ability (and also channel activity) and the mean molecular area at low pressures, e.g., at 10 mN · m^{-1}. The compounds with the largest molecular area (π = 10 mN · m^{-1}) per monomer being the most effective. As is discussed above that the molecular area at low pressures is mainly determined by the possibility of trp–trp interactions, we emphasize in line with several other findings (22–25) the importance of such interactions for the lipid structure modulating effect.

The authors with to thank Dr. D. W. Urry and Dr. K. U. Prasad for the synthesis of the elongated gramicidin derivatives and Dr. F. Heitz for sending us preprints of his recent work.

Received for publication 19 July 1988 and in final form 25 October 1988.

REFERENCES

1. Katz, E., and A. L. Demain. 1977. The peptide antibiotics of *Bacillus:* chemistry, biogenesis, and possible functions. *Bacteriol. Rev.* 41:449–474.
2. Paulus, H., N. Sarkar, P. K. Mukherjee, D. Langley, V. T. Ivanov, E. N. Shepel, and W. Veatch. 1979. Comparison of the effect of linear gramicidin analogs on bacterial sporulation, membrane permeability, and ribonucleic acid polymerase. *Biochemistry.* 18:4532–4536.
3. Mukherjee, P. K., and H. Paulus. 1977. Biological functions of gramicidin: studies on gramicidin negative mutants. *Proc. Natl. Acad. Sci. USA.* 74:780–784.
4. Modest, B., M. A. Marahiel, W. Pschorn, and H. Ristow. 1984. Peptide antibiotics and sporulation: induction of sporulation in asporogenous and peptide-negative mutants of *Bacillus brevis J. Gen. Microbiol.* 130:747–755.
5. Pschorn, W., H. Paulus, J. Hansen, and H. Ristow. 1982. Induction of sporulation in *Bacillus brevis.* 2. Dependence on the presence of the peptide antibiotics tyrocidin and linear gramicidin. *Eur. J. Biochem.* 129:403–407.
6. Andersen, O. S. 1984. Gramicidin channels. *Annu. Rev. Physiol.* 46:531–548.
7. Urry, D. W. 1985. The Enzymes of Molecular Membranes. Vol. 1. A. N. Martonosi, editor. Second ed. Publishing Corp., New York, 229–257.
8. Wallace, B. A. 1986. Structure of gramicidin A. *Biophys. J.* 49:295–306.
9. Rice, D. and E. Oldfield. 1979. Deuterium nuclear magnetic resonance studies of the interaction between dimerystoylphosphatidylcholine and gramicidin A. *Biochemistry.* 18:3272–3279.
10. Chapman, D., B. A. Cornell, A. W. Eliasz, and A. Perry. 1977. Interactions of helical polypeptide segments which span the hydrocarbon region of lipid bilayers. Studies of the gramicidin A lipid water system. *J. Mol. Biol.* 113:517–538.
11. Killian J. A., and B. De Kruijff. 1986. The influence of proteins and peptides on the phase properties of lipids. *Chem. Phys. Lipids.* 40:259–284.
12. Sarges, R., and B. Witkop. 1965. Gramicidin. V. The structure of valine- and isoleucine-gramicidin A. *J. Am. Chem. Soc.* 87:2011–2020.

13. Sarges, R., and B. Witkop. 1965. Gramicidin. VIII. The structure of valine- and isoleucine-gramicidin C. *Biochemistry.* 4:2491–2494.

14. Urry, D. W. 1971. The gramicidin A transmembrane channel: a proposed $\pi_{(L,D)}$ helix. *Proc. Natl. Acad. Sci. USA* 68:672–676.

15. Veatch, W. R., E. T. Fossel, and E. R. Blout. 1974. The conformation of gramicidin A. *Biochemistry.* 13:5249–5256.

16. Veatch, W., and E. R. Blout. 1974. The aggregation of gramicidin A in solution. *Biochemistry.* 13:5257–5264.

17. Sychev, S. V., N. A. Nevskaya, S. Jordanov, E. N. Shepel, A. I. Miroshnikow, and V. T. Ivanow. 1980. The solution conformations of gramicidin A and its analogs. *Bioorg. Chem.* 9:121–151.

18. Wallace, B. A. 1983. Gramicidin A adopts distinctly different conformations in membranes and in organic solvents. *Biopolymers* 22:397–402.

19. Prasad, K. U., T. L. Trapane, D. Busath, G. Szabo, and D. W. Urry. 1983. Synthesis and characterization of (1-13C)Phe gramicidin A. *Int. J. Peptide Protein Res.* 22:341–347.

20. Jones, D., E. Hayon, and D. Busath, 1986. Tryptophan photolysis is responsible for gramicidin-channel inactivation by ultraviolet light. *Biochim. Biophys. Acta.* 861:62–67.

21. Bamberg, E., K. Noda, E. Gross, and P. Lauger. 1976. Single-channel parameters of gramicidin A, B and C. *Biochim. Biphys. Acta.* 419:223–228.

22. Killian, J. A., J. W. Timmermans, S. Keur, and B. De Kruijff. 1985. The tryptophans of gramicidin are essential for the lipid structure modulating effect of the peptide. *Biochim. Biophys. Acta.* 820:154–156.

23. Killian, J. A., K. N. J. Burger, and B. De Kruijff. 1987. Phase separation and induction of H_{II} phase formation by gramicidin A, B and C in dioleoylphosphatidylcholine model membranes. Study on the role of the tryptophan residues. *Biochim. Biophys. Acta.* 897:269–284.

24. Aranda, F. J., J. A. Killian, and B. De Kruijff. 1987. Importance of the tryptophans of gramicidin for its lipid structure modulating activity in lysophosphatidylcholine and phosphatidyl ethanolamine modelmembranes. *Biochim. Biophys. Acta.* 901:217–228.

25. De Kruijff, and J. A. Killian. 1987. Gramicidin A: a molecule on the moves. *Trends Biochem. Sci.* 12:256–257.

26. Boni, L. T., A. J. Conolly, and A. M. Kleinfeld. 1986. Transmembrane distribution of gramicidin by tryptophan energy transfer. *Biophys. J.* 49:122–123.

27. Hinton, J. F., R. E. Koeppe II, D. Shungu, W. L. Whaley, J. A. Paczkowski, and F. S. Millett. 1986. Equilibrium binding constants for Tl^+ with gramicidins A, B and C in a lysophosphatidylcholine environment determined by ^{205}Tl nuclear magnetic resonance spectroscopy. *Biophys. J.* 49:571–577.

28. Urry, D. W., M. C. Goodall, J. D. Glickson, and D. F. Mayers. 1971. The gramicidin A transmembrane channel: characteristics of head to head dimerized $\pi_{(L,D)}$ helices. *Proc. Natl. Acad. Sci. USA.* 68:1907–1911.

29. Urry, D. W., T. L. Trapane, and K. U. Prassad. 1983. Is the gramicidin A transmembrane channel single stranded or double stranded helix? A simple unequivocal determination. *Science (Wash. DC).* 221:1964–1967.

30. Weinstein, S., J. T. Durkin, W. R. Veatch, and E. R. Blout. 1985. Conformation of the gramicidin A channel in phospholipid vesicles: a fluorine-19 nuclear magnetic resonance study. *Biochemistry.* 24:4374–4382.

31. Spisni, A., I. Pasquali-Ronchetti, E. Casali, L. Lindner, P. Cavatorta, L. Masotti, and D. W. Urry. 1983. Supramolecular organization of lysophosphatidylcholine-packaged gramicidin A'. *Biochim. Biophys. Acta.* 732:58–68.

32. Cavatorta, P., A. Spisni, E. Casali, L. Lindner, L. Masotti, and D. W. Urry. 1982. Intermolecular interactions of gramicidin A transmembrane channels incorporated into lysophosphatidylcholine lipid systems. *Biochim. Biophys. Acta.* 689:113–120.

33. Stark, G., M. Strassle, and Z. Takacz. 1986. Temperature-jump and voltage-jump experiments at planar lipid membranes support an aggregational (micellar) model of the gramicidin A ion channel. *J. Membr. Biol.* 89:23–37.

34. Chupin, V., J. A. Killian, and B. De Kruijff. 1987. 2-H Nuclear magnetic resonance investigations on phospholipid acyl chain order and dynamics in the gramicidin-induced hexagonal H_{II} phase. *Biophys. J.* 51:395–405.

35. Killian, J. A., and B. De Kruijff. 1987. Proposed mechanism for H_{II} phase induction by gramicidin in model membranes and its relation to channel formation. *Biophys. J.* 53:111–117.

36. Brasseur, R., J. A. Killian, B. De Kruijff, and J. M. Ruysschaert. 1987. Conformational analysis of gramicidin-gramicidin interactions at the air-water interface suggests that gramicidin aggregates into tube-like structures similar as found in the gramicidin. *Biochim. Biophys. Acta.* 903:11–17.

37. Killian, J. A., and B. De Kruijff. 1985. Thermodynamic, motional and structural aspects of gramicidin-induced hexagonal H_{II} phase formation in phosphatidylethanolamine. *Biochemistry.* 24:7881–7890.

38. Killian, J. A., and B. De Kruijff. 1985. Importance of hydration for gramicidin-induced hexagonal H_{II} phase formation in dioleoylphosphatidylcholine model membranes. *Biochemistry.* 24:7890–7898.

39. Kemp, G., K. A. Jacobsen, and C. E. Wenner. 1972. Solution and interfacial properties of gramicidin pertinent to its effect on membranes. *Biochim. Biophys. Acta.* 255:493–501.

40. Haydon, D. A., and S. B. Hladky. 1972. Ion transport across thin lipid membranes: a critical discussion of mechanisms in selected systems. *Q. Rev. Biophys.* 5:187–282.

41. Kemp, G., and C. Wenner. 1976. Solution, interfacial and membrane properties of gramicidin A. *Arch. Biochem. Biophys.* 176:547–555.

42. Cornell, B. A., M. M. Sacre, W. E. Peel, and D. Chapman. 1978. The modulation of lipid bilayer fluidity by intrinsic polypeptides and proteins. *FEBS (Fed. Eur. Biochem. Soc.) Lett.* 90:29–35.

43. Ries, H. E., and H. Swift. 1987. Monolayers of two transmembrane channel formers and an ionophore. *J. Colloid Interface Sci.* 117:584–588.

44. Davion-Van Mau, N., P. Daumas, D. Lelievre, Y. Trudelle, and F. Heitz. 1987. Linear gramicidins at the air-water interface. *Biophys. J.* 51:843–845.

45. Killian, J. A., C. W. Van den Berg, H. Tournois, S. Keur, A. J. Slotboom, G. J. M. Van Scharrenburg, and B. De Kruijff. 1986. Gramicidin-induced H_{II} phase formation in negatively charged phospholipids and the effect of N- and C-terminal modification of gramicidin on its interaction with zwitterionic phospholipid. *Biochim. Biophys. Acta.* 857:13–27.

46. Urry, D. W., N. Jing, and K. U. Prasad. 1987. On the mechanism of channel-length dependence of gramicidin single-channel conductance. *Biochim. Biophys. Acta.* 902:137–144.

47. Westfall, F. C., J. Scotchler, and A. B. Robinson. 1972. The use of propionic acid-hydrochloric acid hydrolysis in Merrifield solid-phase peptide synthesis. *J. Org. Chem.* 37:3363–3365.

48. Van Deenen, L. L. M., and G. H. De Haas. 1964. The synthesis of

phosphoglycerides and some biochemical applications. *Adv. Lipid Res.* 2:168–229.

49. Dekker, C. J., W. S. M. Geurts van Kessel, J. P. G. Klomp, J. Pieters, and B. De Kruijff. 1983. Synthesis and polymorphic phase behaviour of polyunsaturated phosphatidylcholines and phosphatidylethanolamines. *Chem. Phys. Lipids.* 33:93–106.
50. Fiske, C., and Y. Subbarow. 1925. The colorimetric determination of phosphorus. *J. Biol. Chem.* 66:375–400.
51. Benjamins, J., J. A. De Feyter, M. T. A. Evans, and M. C. Phillips. 1975. Dynamic and static properties of proteins at the air/water interface. *Trans. Faraday Soc.* 71:375–383.
52. Gieles, P. M. C. 1987. Methods of measurements for the evaluation of monolayer properties. Ph.D. thesis. Eindhoven University of Technology, The Netherlands.
53. Boonman, A., P. M. C. Gieles, C. H. Massen, and J. Egberts. 1985. Dynamic surface tension measurement on surface active materials. *Thermochim. Acta.* 103:107–110.
54. Lucassen-Reynders, E. H., and J. Lucassen. 1969. Properties of capillary waves. *Adv. Colloid Interface Sci.* 2:347–367.
55. Lucassen, J. 1968. Longitudinal capillary waves. Part 1. Theory. *Trans. Faraday Soc.* 64:2221–2229.
56. Van den Tempel, M., and E. H. Lucassen-Reynders. 1983. Relaxation processes at fluid interfaces. *Adv. Colloid Interface Sci.* 18:281–301.
57. Blank, M., J. Lucassen, and M. Van den Tempel. 1977. The elasticities of spread monolayers of bovine serum albumin and of ovalbumin. *J. Colloid Interface Sci.* 33:94–100.
58. Graham, D. E., and M. C. Phillips. 1979. Proteins at liquid interfaces. III. Molecular structures of adsorbed films. *J. Colloid Interface Sci.* 70:427–439.
59. Graham, D. E., and M. C. Phillips. 1980. Proteins at liquid interfaces. *J. Colloid Interface Sci.* 76:227–239.
60. Malcolm, B. R. 1968. Molecular structure and deuterium exchange in monolayers of synthetic polypeptides. *Proc. Roy. Soc. A.* 305:363–385.
61. Tournois, H., J. A. Killian, D. W. Urry, O. R. Bokking, J. De Gier, and B. De Kruijff. 1987. Solvent determined conformation of gramicidin affects the ability of the peptide to induce H_{II} phase formation in dioleoylphosphatidylcholine model membranes. *Biochim. Biophys. Acta.* 905:222–226.
62. Killian, J. A., K. U. Prasad, D. Hains, and D. W. Urry. 1988. The membrane as an environment of minimal interconversion. A circular dichroism study on the solvent dependence of the conformational behavior of gramicidin in dioleoylphosphatidylcholine model membranes. *Biochemistry.* 27:4848–4855.
63. Brasseur, R., V. Cabiaux, J. A. Killian, B. De Kruijff, and J. M. Ruysschaert. 1986. Orientation of gramicidin A at the lysophosphatidylcholine/water interface: a semi-empirical conformational analysis. *Biochim. Biophys. Acta.* 855:317–324.
64. Killian, J. A., B. De Kruijff, C. J. A. Van Echteld, A. J. Verkley, J. Leunissen-Bijvelt, and J. De Gier. 1983. Mixtures of gramicidin and lysophosphatidylcholine form lamellar structures. *Biochim. Biophys. Acta.* 782:141–144.
65. Macdonald, P. M., and J. Seelig. 1988. Dynamic properties of gramicidin A in phospholipid membranes. *Biochemistry.* 27:2357–2364.
66. Killian, J. A., F. Borle, B. De Kruijff, and J. Seelig. 1986. Comparative ^{2}H- and ^{31}P-NMR study on the properties of palmitoyllysophosphatidylcholine in bilayers with gramicidin, cholesterol and dipalmitoylphosphatidylcholine. *Biochim. Biophys. Acta.* 854:133–142.